

All-to-all reconfigurability with sparse and higher-order Ising machines

Srijan Nikhar,^{1,2,*} Sidharth Kannan,^{1,2} Navid Anjum Aadit,^{1,2} Shuvro Chowdhury,¹ and Kerem Y. Camsari^{1,†}

¹*Department of Electrical and Computer Engineering,
University of California, Santa Barbara, Santa Barbara, CA, 93106, USA*

²*Equally contributing authors*

(Dated: May 24, 2024)

Domain-specific hardware to solve computationally hard optimization problems has generated tremendous excitement recently. Here, we evaluate probabilistic bit (p-bit) based on Ising Machines (IM) or p-computers with a benchmark combinatorial optimization problem, namely the 3-regular 3-XOR Satisfiability (3R3X). The 3R3X problem has a glassy energy landscape, and it has recently been used to benchmark various IMs and other solvers. We introduce a multiplexed architecture where p-computers emulate all-to-all (complete) graph functionality despite being interconnected in sparse networks, enabling a highly parallelized chromatic Gibbs sampling. We implement this architecture in FPGAs and show that p-bit networks running an adaptive version of the powerful parallel tempering algorithm demonstrate competitive algorithmic and prefactor advantages over alternative IMs by D-Wave, Toshiba, and Fujitsu, except a greedy algorithm accelerated on a GPU. We further extend our APT results using higher-order interactions in FPGAs and show that while higher-order interactions lead to prefactor advantages, they do not show any algorithmic scaling advantages for the XORSAT problem, settling an open conjecture. Even though FPGA implementations of p-bits are still not quite as fast as the best possible greedy algorithms implemented in GPUs, scaled magnetic versions of p-computers could lead to orders of magnitude over such algorithms according to experimentally established projections.

I. INTRODUCTION

Ising machines and domain-specific accelerators for hard optimization problems have generated tremendous interest lately. Different implementations using various physics-inspired approaches have been implemented using a range of physical substrates (see Ref. [1] for a comprehensive review). Unlike D-Wave’s quantum Ising machines that operate with sparse connectivity, most recent Ising machines have emphasized all-to-all network topologies [2–5], motivated by the ease of reconfigurability. While all-to-all topology eases programming different instances of optimization problems expressed as Ising Hamiltonians, in our view, this is a temporary solution [6] since the $\mathcal{O}(n^2)$ dependence of weights will be unsustainable at large scales. The scaling problem becomes even harder if the all-to-all Hamiltonians include higher-order terms $\mathcal{O}(n^k)$, where k is the locality of the Hamiltonian. As such, some form of sparsification or sparse-problem embedding seems unavoidable.

In this work, we focus on an emerging, physics-inspired solver based on probabilistic bits (p-bit), emphasizing *sparse*, *massively parallel*, and *reconfigurable* architectures capable of realizing higher-order interactions. p-bits are inspired by the statistical physics of interacting particles encountered in nature (Figure 1a) where particles form sparsely connected, asynchronous, and massively parallel networks (Figure 1b). Sparsity enables a large degree of concurrency by allowing large parts of networks to be updated in parallel without introducing any errors, unlike densely connected networks that need to be updated serially [7, 8]. However, sparse and fixed topologies cannot be easily reconfigured; they lack the flexibility provided by all-to-all architectures. We solve this

problem by introducing a reconfigurable architecture while *holding on to the massive parallelism* of sparse networks. Our central idea is to introduce a master graph architecture that can multiplex different connectivity and phase-shifted (colored) clocks for a given p-bit to enable reconfigurability and parallelism. We also introduce the first implementation of third-order interactions in a large-scale FPGA-based p-computer. We implement both of these concepts in Field Programmable Gate Arrays (FPGA) and compare our implementation on a recently introduced combinatorial optimization challenge, namely the XORSAT problem [9, 10] (Figure 1c). Our FPGA-based p-computer uses a sophisticated heuristic algorithm called adaptive parallel tempering (APT) [11, 12]. PT (Figure 1d) maintains replicas of a given network at different computational temperatures, which exchange states at regular intervals. Unlike simulated annealing, PT never permanently gets stuck in local minima. Variations of PT are considered to be the most powerful heuristic algorithms of unstructured optimization problems [13]. The “adaptive” version of PT we adopt here uses a problem-dependent preprocessing step in order to identify the optimum number of replicas and temperature profiles, avoiding bottlenecks during replica swaps.

With reasonable assumptions and experimental demonstrations, we show that FPGA-based p-computers running the APT algorithm exhibit extremely competitive hardware and algorithmic scaling compared to leading IMs [4, 14–17]. We demonstrate that going from a 2-body to a 3-body realization of the XORSAT problem results in a significant prefactor advantage on the time to solution and halves the number of p-bits but results in no improvement to scaling, settling a conjecture posed in [10]. Moreover, projections based on nanodevices such as stochastic magnetic tunnel junctions (sMTJ) show that scaled p-computers could deliver unprecedented advantages in hard optimization without suffering from reconfigurability issues.

* srijannikhar@ucsb.edu

† camsari@ece.ucsb.edu

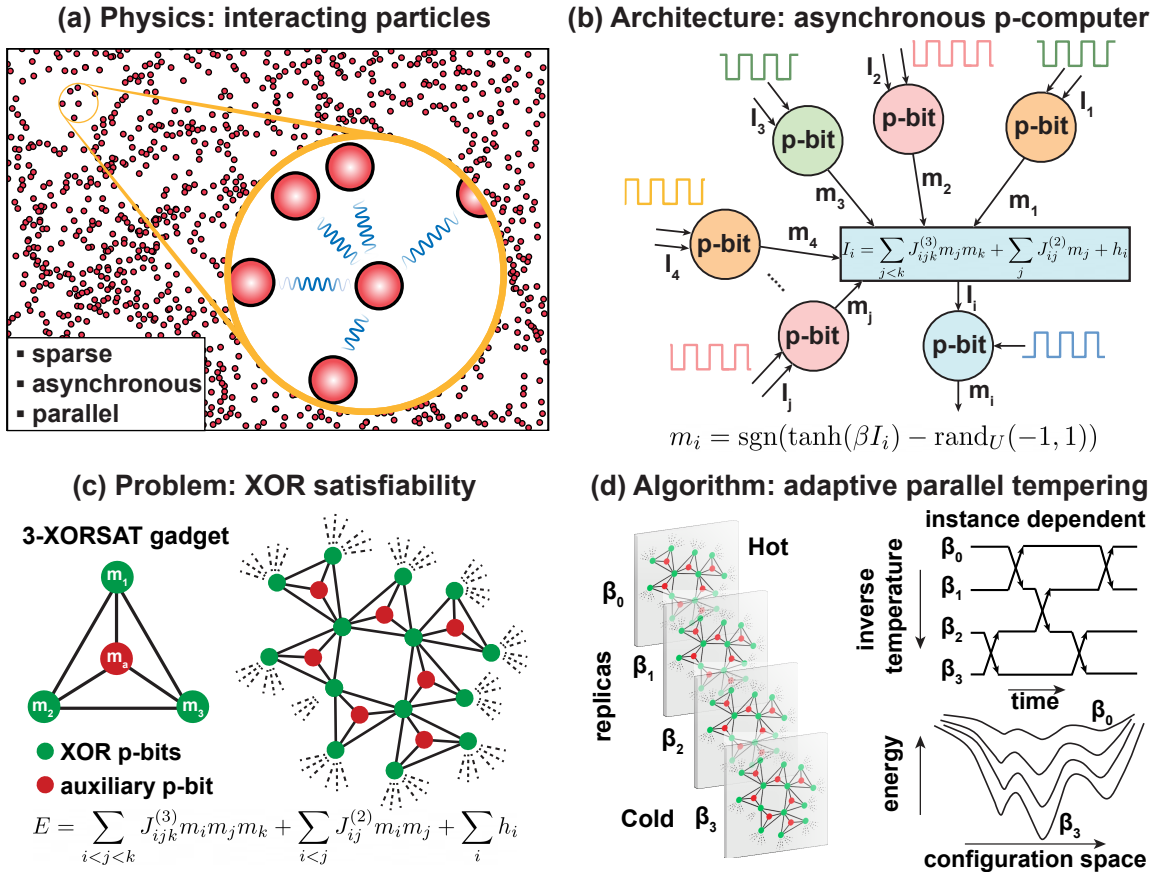


Fig. 1. a) Many-body physics of interacting particles have local connectivity (sparse), asynchronous dynamics (clockless), and massive parallelism. b) Asynchronous p-computers take inspiration from the physics of (a). Each p-bit asynchronously (shown with phase-shifted clocks) receives input from local neighbors followed by probabilistic activation. c) The 3-regular 3-XORSAT (3R3X) problem [9, 10] under study. d) We use the adaptive parallel tempering (APT) algorithm [11, 12] on FPGA-based p-computers to solve the 3R3X problem. APT uses replicas of the original network, operated at different computational temperatures where neighboring replicas swap their states based on a Metropolis criterion at regular intervals.

We organize the rest of the paper as follows: we first discuss the background of p-computing, followed by our multiplexed sparse network that emulates all-to-all reconfigurability on quadratized instances, with experimental results establishing how our multiplexed architecture retains its massive parallelism without any degradation in solution quality. We then discuss how the massive parallelism provides an $\mathcal{O}(n)$ scaling advantage over serial all-to-all solvers. We extend this discussion to the multiplexed hardware implementation of third-order interactions in our digital p-computers and show how such an architecture-based scaling advantage extends to higher-order p-computers. Finally, we benchmark the XORSAT challenge in our digital p-computers and compare the performance of our second and third-order implementations against those of other leading Ising Machines.

II. RESULTS AND DISCUSSION

A. Background on p-bits and XORSAT

The dynamics of p-computers can be described as a discrete Markov Chain Monte Carlo (MCMC) algorithm, known as Gibbs sampling or Glauber dynamics [18]. For each p-bit in the network, we have:

$$I_i = \sum_j J_{ij} m_j + h_i \quad (1)$$

$$m_i = \text{sgn} [\tanh(\beta I_i) - \text{rand}_U(-1, 1)] \quad (2)$$

where $m_i \in \{-1, +1\}$ and $\text{rand}_U(-1, 1)$ is a uniform random number that lies in the interval $[-1, 1]$. $\{J_{ij}\}$ and $\{h_i\}$ correspond to the weights and biases respectively. β is the inverse temperature. After a sufficient number of iterations, Eq. 2 approximates the Boltzmann distribution [8] given by:

$$p(\{m\}) = \frac{1}{Z} \exp[-\beta E(\{m\})] \quad (3)$$

$$E(\{m\}) = - \sum_{i<j} J_{ij} m_i m_j - \sum_i h_i m_i \quad (4)$$

where Z is the partition function. Generalizations of the Ising Hamiltonian (Eq. 4) beyond quadratic terms are possible and have been implemented previously [19–26]. One such generalization that we implement in our p-computers is the inclusion of third-order interactions implemented by modifying Eq. 1 to:

$$I_i = \sum_{j < k} J_{ijk}^{(3)} m_j m_k + \sum_j J_{ij}^{(2)} m_j + h_i \quad (5)$$

while keeping Eq. 2 the same. Here $\{J_{ijk}^{(3)}\}$ models the third-order interaction, whereas $\{J_{ij}^{(2)}\}$ models the second-order interaction.

Eqs. 1-2, and 5 are extremely general and can be used to solve a wide variety of problems in optimization, sampling (for energy-based machine learning) and quantum simulation through quantum Monte Carlo [28] and variational quantum machine learning algorithms [29]. Here, we focus on the 3R3X problem, which encodes clauses of the type $C_k = (x_i \oplus x_j \oplus x_k)$, typically mapped to quadratic Ising energies via auxiliary variables (Figure 1c), however, in this paper, we also implement a native third-order mapping without any auxiliary variables. This is a benchmark problem with a golf-course-like energy landscape that is difficult for heuristic Monte Carlo solvers to tackle [35] even though it admits a polynomial time algorithm through its relation to a system of linear equations modulo 2, which can be solved by Gaussian elimination [17]. Nonetheless, the problem resembles hard generic SAT problems, and slight variations of it cannot be solved by Gaussian elimination and its main value is to serve as a benchmark for hard optimization problems and Ising solvers.

B. Adaptive Parallel Tempering

Our p-computers run an adaptive version of the parallel tempering (APT) algorithm, in which multiple replicas of the same p-bit network are run at different temperatures in parallel (according to Eq. 2-Eq. 5) and then periodically swapped with swap probability defined by the Metropolis criterion:

$$P_{sw} = \min(1, e^{-\Delta E \Delta \beta}) \quad (6)$$

where P_{sw} is the probability of swapping the temperatures of 2 adjacent replicas, ΔE and $\Delta \beta$ are the differences in the energies and inverse temperatures of these adjacent replicas. This swapping enables the solver to avoid getting trapped in local minima, as high-temperature replicas explore the whole energy landscape while lower-temperature replicas exploit the most promising paths through it. The APT algorithm determines a temperature profile specific to each problem, as described in Algorithm 1. It was, however, found that the temperature profiles generated using the APT preprocessing algorithm lead only to very slight variations over all 100 XORSAT instances of a certain problem size. Therefore, for a given problem size, a fixed temperature profile generated using a randomly chosen instance of the corresponding problem size was used in all our experiments.

C. All-to-All Reconfigurability via Sparse Network Multiplexing

We define all-to-all reconfigurability as the ability to solve multiple instances of a given problem using the same hardware. We implement a *dense* master graph architecture on both second-order and third-order problems that can be multiplexed to access different instances of a *sparse* combinatorial optimization problem. While our approach cannot fully emulate all-to-all reconfigurability on natively dense problems, it has previously been shown how such problems can efficiently be sparsified while leveraging a large degree of parallelism [7]. Concretely, our approach is based on combining all 100 sparse instances of the 3R3X problem (as defined in the XORSAT challenge) into a single master graph that allows activating one instance at a time (Figure 2). In general, a master graph can be defined as a complete graph that can house different instances of a sparsified optimization problem, either statically multiplex (as in this paper) or dynamically reconfigured (to activate any desired instance). As we discuss in the following sections, the master graph approach must also multiplex the *colors* of a given node, which selects phase-shifted clocks for sparse p-bit networks that are updated in large parallel blocks.

1. Instance Reconfiguration

Choosing instances one at a time requires the master graph nodes to be reconfigurable to multiplex changing neighbors over different instances. (Figure 2a). Therefore, all *potential* neighbors of a given p-bit over different instances need to be known previously to be multiplexed using a neighbor multiplexer (Figure 2b).

2. Clock (Color) Reconfiguration

Our p-computer employs graph-colored [30] Gibbs sampling to achieve massive parallelism [7] by updating blocks of unconnected p-bits at the same time, using Eq. 1-2 and 5. The 3R3X instances are naturally sparse, and graph coloring their graph representation requires a maximum of 6 colors. Since only one instance is selected at a time, the master graph needs only 6 phase-shifted clocks. However, the color of a particular p-bit on the master graph can vary across instances and needs to be multiplexed as well (Figure 2b). The phase-shifted clock signals are multiplexed using the instance selection signal before being supplied to the p-bits. In our master graph implementation, all possible weights for a given p-bit are not stored on-chip (inside the FPGA), but they are simply reprogrammed into the FPGA along with the instance selection signal from a CPU (note that this does not require any resynthesis). For a truly standalone master graph architecture, the weights can be stored in on-chip memory and loaded to solve a given instance.

For the weights (J_{ij}) that are modulated by the computational inverse temperature β , we have chosen a fixed-point precision: 1 bit for the sign, 6 bits for the integer part, and 6 bits for the fraction part, i.e., $s\{6\}\{6\}$. This optimal bit-precision was carefully chosen by comparing the master graph results against the CPU as shown in Figure 2c-e. All our

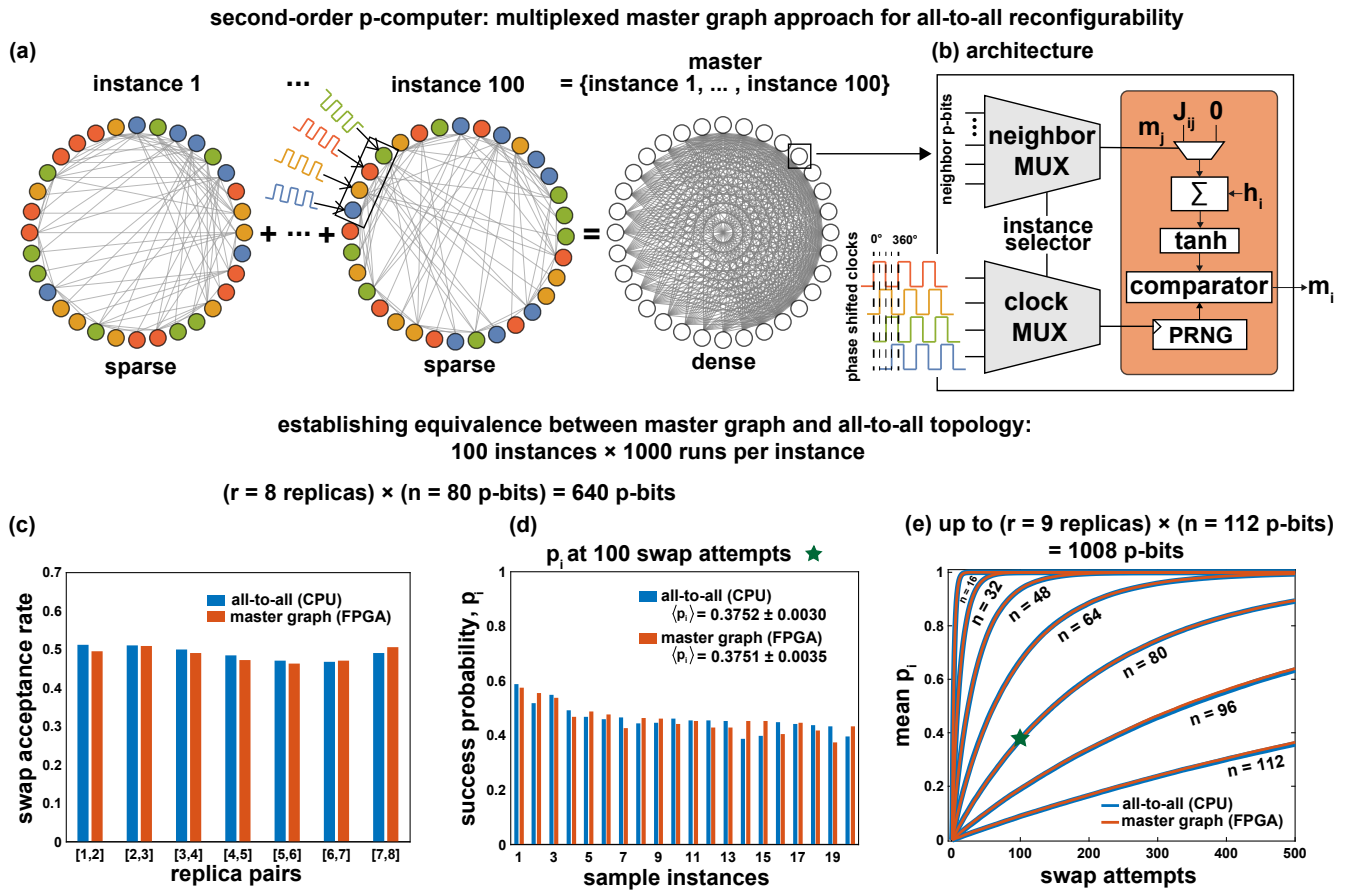


Fig. 2. a) For each problem size (n), multiple graph-colored sparse instances of the 3R3X problem are combined to form a dense master graph. b) Reconfigurable master graph architecture: neighbors and clocks for each p-bit are multiplexed using an instance selector. c) Establishing equivalence between master graph (FPGA) and all-to-all graph (CPU): pair-wise swap acceptance rates showing roughly equal probability obtained from APT across 8 replicas for $n = 80$. d) 20 instances with the highest success probabilities (p_i) are shown for $n = 80$. All p_i values are computed from 1000 independent runs. e) Mean p_i as a function of swap attempts at varying n .

FPGA results in this work have been implemented on a single Xilinx Alveo U250 FPGA. Each phase-shifted p-bit clock is a 15 MHz clock generated in the FPGA. The random numbers required for emulating Eq. 2 are obtained using Xoshiro [31] as the pseudo-random number generator.

3. Establishing Equivalence between Master and All-To-All Topology

We performed a statistical analysis using the APT algorithm described in Algorithm 1 on 3R3X instances to verify master graph implementations on FPGA and compared our results with the all-to-all CPU implementation. It was ensured that both CPU and FPGA used the same APT parameters for our experiments. The temperature profiles and the number of replicas for each problem size were determined using the APT preprocessing step described as part of Algorithm 1. The parameters used for preprocessing were set to $\alpha = 1$, $\beta_0 = 1.0$, $\sigma_{\min} = 0.5$, $N_{\text{chains}} = 100$, $L = 2000$. Each replica used for this experiment is an individual master graph that includes all 100 instances multiplexed together. For each problem size, all the replicas were fit in the same FPGA synthesis, and the clock multiplexers were

shared between them.

In all our experiments, 100 Monte Carlo (MC) sweeps were performed between 2 successive swap attempts. In this work, we define a sweep as when all the p-bits in the network (across all replicas) have attempted to flip once, as these occur in parallel in our hardware. For every problem size, APT was run on each of the 100 instances for 1000 runs, allowing us to obtain a success probability, p_i , for each instance. Since the ground state energy of these problems is known, before every swap attempt, the energy of every replica is calculated and compared against the ground state. The run is considered successful if any one of the replicas reaches the ground state, after which the run is terminated, and the number of swap attempts required to reach the ground state is noted. Note that this measurement approach allows an estimation of p_i serving as validation experiments; however, in Section II F, we will use p_i to estimate actual time to solution metrics.

Figure 2c shows pairwise swap acceptance probabilities for an 8 replica, 640 p-bit system corresponding to $n = 80$. Roughly uniform replica swap probabilities are observed, indicative of how the APT algorithm creates efficient temperature profiles, similar to the PT variant used for DAU

Algorithm 1: Adaptive Parallel Tempering with p-computers

Input: Weights, biases, number of swaps, sweeps per swap, colormap, step rate, initial temperature, energy variance tolerance, number of chains, sweeps per chain

Output: State corresponding to minimum energy, m_{opt}

```

1 Function p-computer (weights, biases, colormap, temp.):
2   for each color in the colormap do
3     for each p-bit in the color do
4       solve Eq. 1 and Eq. 2
5    $t \leftarrow 0$ 
6   initialize all parallel chains to random states
7   while energy variance is greater than tolerance do
8     for each chain in parallel do
9       for each sweep do
10        sample p-bit states from p-computer
11        compute energy of the chain
12        Compute energy variance for the chain
13        save the p-bit states
14    compute mean energy variance of chains,  $\sigma_E$ 
15     $\beta_{t+1} \leftarrow \beta_t + \frac{\alpha}{\sigma_E}$ ,  $t \leftarrow t + 1$ 
16 initialize all replicas to random states
17 for each swap attempt do
18   if it is an even-numbered swap attempt then
19     choose (even, odd) sequential pairs
20   else
21     choose (odd, even) sequential pairs
22   for each replica in parallel do
23     for each sweep do
24       sample p-bit states from p-computer
25       compute the energy of the replica
26   for each sequential pair of replicas do
27     propose a swap
28     if accepted then
29       swap the p-bit states between the replicas
30 return p-bit states for the replica with the minimum energy

```

[10].

Figure 2d compares success probabilities over sample instances between the all-to-all (CPU) and master graph (FPGA) approach for $n = 80$. Over 100 instances, the mean success probabilities between CPU and FPGA match up to 3 decimal places (errors calculated from maximum deviations at 95% confidence intervals). Finally, Figure 2e shows mean success probabilities over all instances as a function of swap attempts between the CPU and the FPGA with excellent agreement.

Overall, the results in Figure 2c-e establish the equivalence of our master graph approach with the all-to-all topology in CPU and verify our master graph implementation in the FPGA that achieves reconfigurability without sacrificing the massive parallelism (as we later show in Fig. 3b where the time to sample a full network stays constant across increasing

problem sizes).

D. Architecture-Enabled Scaling Advantage of p-computers

Figure 3a shows the algorithmic complexity of the 3R3X problem using the APT algorithm, independent of the all-to-all (CPU) and master graph (FPGA) implementations. While Figure 3 presents the results produced on the second-order implementation, this analysis is also extended to the third-order problems in the following sections. We report the optimal median sweeps to solutions for different instance sizes running APT to solve 100 instances per size with 1000 runs per instance. For the all-to-all (CPU) approach, we have data for all the problem sizes; however, for the master graph (FPGA) approach, we have data points up to 112 bits, which is the largest we could fit on our single FPGA. The detailed methodology of the optimal median sweeps computation is discussed in Section IV C. The CPU and the FPGA data fall on top of each other, showing hardware independence and the raw algorithmic complexity despite the significant differences in the CPU implementations using float64 precision and more sophisticated RNGs (Mersenne) compared to Xoshiro. In Figure 3b, we report the average time required to compute each sweep for both CPU and FPGA. The CPU's computation time escalates with the problem size showing $\mathcal{O}(n)$ scaling despite using the same optimized graph-coloring algorithm for block updates. Conversely, the FPGA's computation time remains constant since all the replicas and color blocks operate in parallel. This parallelism enables a linear increase in flips per second, resulting in an $\mathcal{O}(n)$ improvement for the FPGA over the CPU due to our architecture. Multiplying the optimal median sweeps from Figure 3a by the average time per sweep from Figure 3b, we calculate the optimal median time to solution (Eq. 7) in seconds in Figure 3c. These architectural benefits are not confined to second-order implementations. In subsequent sections, we demonstrate how similar advantages were also realized in higher-order p-computers.

E. Higher-Order Interactions

The 3 spin clauses of the 3R3X instances make them suitable to be represented by cubic Ising interactions. In cubic form, XORSAT problem instances need only one spin per SAT variable, without any auxiliary spins [9]. This halves the total number of the p-bits required to represent a particular problem. The details of this reduction are mentioned in Section IV A. To evaluate the performance of the 3R3X instances in their native third-order form, we extended the master-graph implementation discussed in Section II C to implement a reconfigurable third-order p-computer. The following sections discuss the details of hardware implementation for our third-order p-computer.

1. Hypergraph Coloring

To preserve the massive parallelism for third-order problems, we need to extend the idea of graph-colored Gibbs sampling. Higher-order Ising systems can be represented as *hypergraphs*, which model multi-spin interactions as nodes

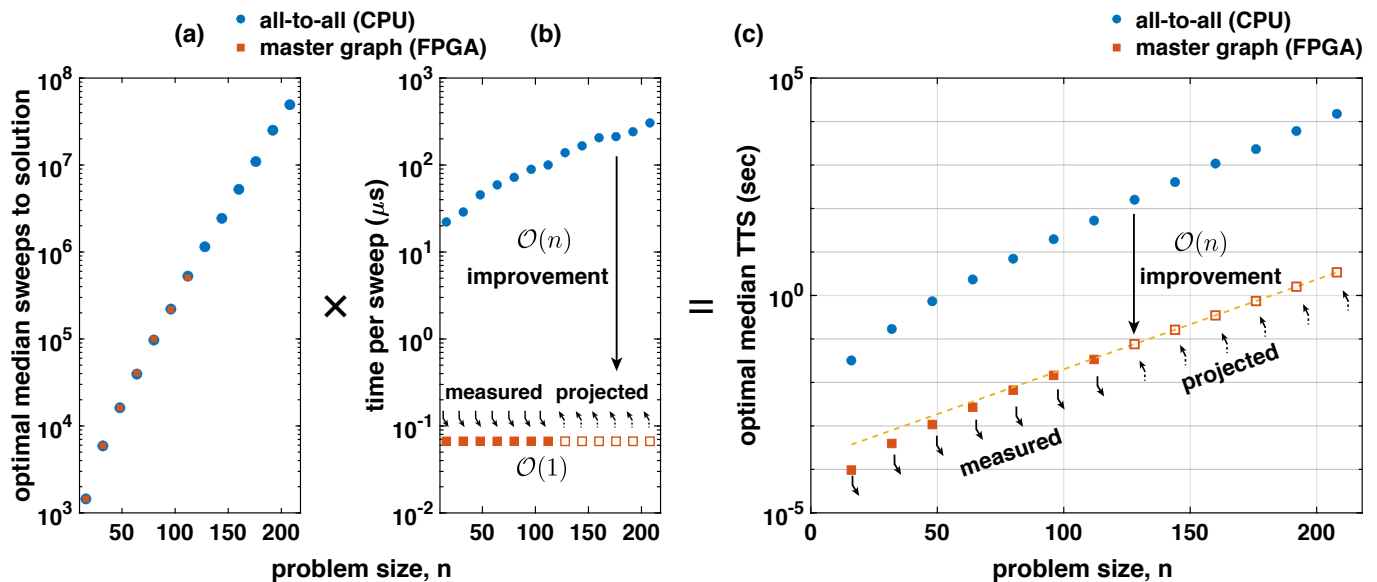


Fig. 3. a) The algorithmic complexity of the 3R3X problem as a function of Monte Carlo (MC) sweeps to the solution, independent of all-to-all (CPU) or master graph (FPGA) implementation. b) The average time to complete one MC sweep is shown for both CPU and FPGA. For CPU, we observe an $\mathcal{O}(n)$ dependence as in [10]. For the master graph, we observe an $\mathcal{O}(1)$ dependence. c) Multiplying (a) with (b) yields time to solution (TTS), preserving the $\mathcal{O}(n)$ improvement over the CPU (see [28] for a similar analysis).

connected in n -tuples. As in the two-body case, the XORSAT hypergraphs are sparse, with each spin being in at most three clauses, enabling a massively parallel architecture using hypergraph-colored p-bits. Extending from quadratic interactions, we enforce the strong hypergraph coloring constraint, in which two nodes that share a hyper-edge must be different colors. This creates the restriction that even in a multi-spin interaction, no two interacting nodes can update in parallel. To produce a strong hypergraph coloring, it is sufficient to color the 2-body clique graph, which, in the case of the XORSAT problem, is equivalent to the 2-body form of the problem, with all auxiliary spins removed. Thus, the same color assignments from the 2-body problem instances can be used here. In Fig. 4, we demonstrate that such a coloring still converges to the Boltzmann distribution, while the weaker restriction that each clause must contain ≥ 2 colors produces a different stationary distribution.

2. Hardware Architecture

The hardware architecture for modeling third-order Ising interactions is similar to the one used for quadratic Hamiltonians [7], except for a slight modification in the multiply-accumulate (MAC) unit to accommodate the third-order terms of Eq. 5. Because the FPGA employs binary spins, only the terms where both m_j and m_k are equal to 1 contribute to Eq. 5. This scenario can be efficiently handled using a multiplexer that directs the weights to the accumulator exclusively when both associated spins are 1 (Figure 5). Such an implementation is highly general and can be extended to incorporate arbitrarily higher-order interaction terms.

The third-order master-graph implementation also builds upon the approach mentioned in section II C. For every p-bit, neighbors exist in pairs and must be multiplexed accordingly.

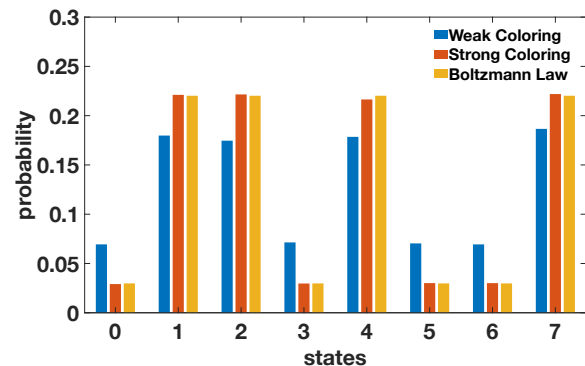


Fig. 4. Fully connected XORSAT clause: Comparison between strong hypergraph coloring, weak hypergraph coloring, and Boltzmann Law, using 10^5 samples. In a weak coloring, where two p-bits in the same clause can be the same color, the network does not reach the Boltzmann distribution.

We also established the equivalence between the all-to-all CPU and reconfigurable FPGA implementations using the same experiments used for the second-order implementation as shown in Figures 6 a-c. The advantages of massive parallelism are achieved by clock multiplexing using the hypergraph coloring procedure discussed in Section II E 1. Thus, the hardware implementation for the third-order p-computer also gives an $\mathcal{O}(n)$ advantage over the CPU implementation. This is illustrated in Figures 6 d-f.

F. p-computer Results on the XORSAT Challenge

Next, we present results using p-computers on the XORSAT challenge (Figure 7), established by Kowalsky *et*

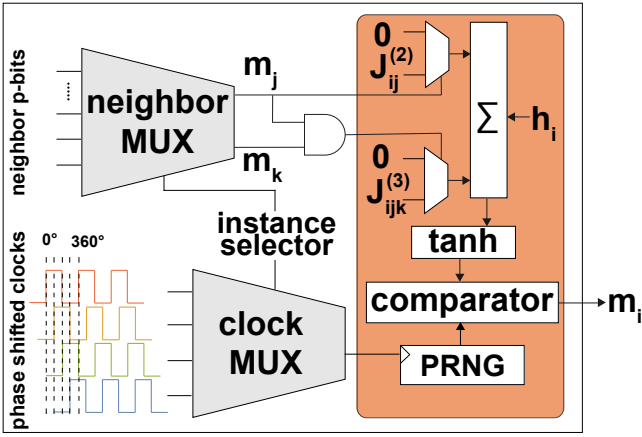


Fig. 5. Hardware architecture for higher order master graph. Weights are selected using two multiplexers, one identical to the weight selector in the 2-body design and the other controlled by two neighboring spins passed through an AND gate. The binary nature of p -bits greatly simplifies the higher-order interactions, avoiding multiplications.

al. [10]. We report measured data for the FPGA-based probabilistic computer’s optimal median time to solution across a range of problem sizes from 16 to 112 for second-order implementation, whereas from 16 to 160 for third-order implementation, with projected performance for the remaining sizes up to 208 based on the CPU data.

The optimal median time to solution is defined as [10]:

$$\langle \text{TTS} \rangle_q = \min_{t_f} \left\langle t_f \frac{\ln(1 - 0.99)}{\ln[1 - p_i(t_f)]} \right\rangle_q \frac{1}{f_p(n)} \quad (7)$$

where q represents the median ($q = 0.5$), the first ($q = 0.25$) and the second quartiles ($q = 0.75$) of TTS over the instances. $f_p(n)$ is a parallelization factor that counts how many runs of the same instance can be executed in parallel in a single solver. Even though we could fit multiple master graphs at lower n , we used $f_p = 1$ for the FPGA-based p -computer at all n . Figure 7 focuses on the median optimal TTS, i.e., $\langle \text{TTS} \rangle_{q=0.5}$ for all solvers and Table I reports the scaling exponent γ and the prefactor η for each quartile. A detailed description of TTS calculation is mentioned in Section IV C

The optimal median TTS for each solver is modeled against the size of the 3R3X instance n by the relationship [10]:

$$\langle \text{TTS} \rangle_q \sim 10^{\gamma n + \eta} \quad (8)$$

1. Second-Order Implementation

Our FPGA-based p -computer’s performance is reflected by a consistent slope of 0.0206, as a result of the constant average sweep time of the FPGA irrespective of problem size discussed in Figure 3. It is interesting to note that the instance-dependent adaptive PT algorithm running on our FPGA-based p -computer shows improvements in both γ and η over the standard PT results reported in [10], nearly matching the performance of the PT-based DAU solver [5]. The reason

for this improvement is the highly efficient graph-colored architecture [7] in our FPGA, where the entire network is updated in one clock cycle ($T_{\text{clk}} = 66.67$ ns). Without this architecture-enabled scaling advantage, the slopes with our APT and the PT [10] are roughly the same; however, the APT uses fewer replicas at all sizes, e.g., 11 replicas at $n = 208$, as opposed to 32 in PT. Note that we have only used a single instance at a given size to create the temperature profiles, and further improvements are possible with hyperparameter optimization on different instances. Kowalsky *et al.* originally grouped the solvers into three groups based on scaling: (i) SATonGPU and DAU, (ii) SBM, PT and MEM, (iii) DWA where only two of the solvers represent dedicated hardware: DWA and DAU. The second-order p -computer (FPGA) shows a close performance to the leading group of solvers in (i) while outperforming (ii) and (iii) as seen in Table I and Figure 7a. Moreover, our third-order implementation outperforms every solver except for SATonGPU, as illustrated through Figure 6 and the related discussion in the following section.

2. Third-Order Ising Machines

Figure 7b illustrates the performance of our third-order p -computer with other solvers. Similar to Figure 7, this figure is also adapted from [10]. To facilitate the comparison with other solvers, the x-axis represents problem sizes in terms of second-order instance sizes as in [10]. Therefore, all third-order instance sizes are scaled by a factor of 2. This is also followed in all references to problem size (n) for third-order instances in this manuscript.

Compared with the benchmarks for the second-order p -computer in Fig 7a, a performance improvement is clearly evident in terms of the prefactor (Table I). The third-order p -computer (FPGA) outperforms the DAU with this prefactor advantage. However, a slope of 0.0201 matches that of the second-order implementation for up to 3 decimal places. Thus, even though a prefactor advantage is seen in the third-order form, no significant improvement in scaling is observed. Even though the APT algorithm is not purely a local solver, the lack of algorithmic improvement may indicate the scaling is near-optimal, as discussed in Ref. [17]. At first sight, the quadratization of the natively third-order energy landscape may suggest it introduces severe difficulties for a Monte Carlo algorithm. Auxiliary spins extend the phase space exponentially, and transitions between viable solutions of clauses are hindered by additional barriers, energetic and entropic. Surprisingly, however, these “disadvantages” do not always lead to a scaling difference for an algorithm: the Adaptive Parallel Tempering we employ in this work shows identical scaling for the second and third-order formulation of the XORSAT problem with minor differences limited to prefactors. Thus, we conclude that even when an optimization problem is natively k -order, a k -local formulation may not lead to improved scaling. In the case of XORSAT, our results settle an open conjecture by Kowalsky *et al.* [10] regarding whether a third-order formulation would improve scaling exponents and may indicate an optimal scaling achieved by the APT algorithm, as suggested by Bernaschi *et al.* [17].

It is important to note that we used a single FPGA unit

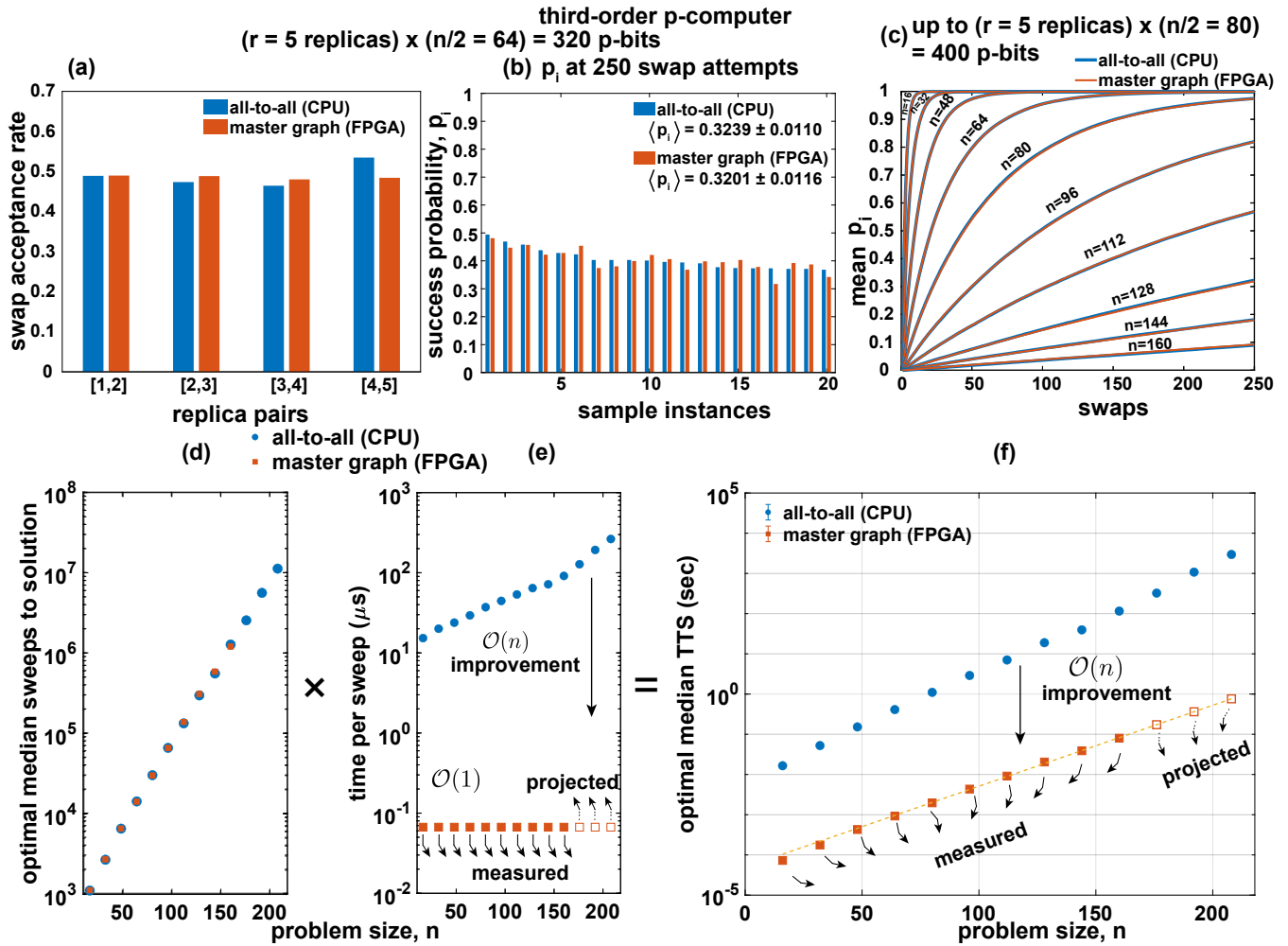


Fig. 6. Performance comparison between CPU and FPGA implementations of third-order p-computers. a) A roughly equal replica swap probability for 5 replicas of problem size $n = 128$ indicates a good temperature profile generated during APT. b) The performance comparison of CPU with FPGA in terms of success probability of individual instances after 250 swap attempts and c) across multiple problem sizes in the range of 0 to 250 swap attempts indicate a clear overlap between the CPU and the FPGA. d) This overlap in algorithmic performance is visible in optimal median sweeps-to-solution as well. e) An $\mathcal{O}(n)$ performance advantage over CPU is observed in sweep times, which is translated to f) an overall performance benefit in the FPGA implementation of third-order p-computer.

TABLE I. We reproduce data from Table 2 of Ref. [10] and add the corresponding numbers obtained for FPGA-based p-computers (highlighted in blue). Lower constants (γ, η) indicate better scaling and better prefactors, respectively.

Solver	γ			η		
	$q = 0.25$	$q = 0.5$	$q = 0.75$	$q = 0.25$	$q = 0.5$	$q = 0.75$
SATonGPU	n/a	0.0171(7)	n/a	n/a	-5.9(3)	n/a
DAU	0.0181(2)	0.0185(4)	0.0190(4)	-3.51(4)	-3.56(7)	-3.49(7)
SBM	0.0211(7)	0.0217(6)	0.0234(8)	-2.6(2)	-2.6(1)	-2.7(1)
PT	0.0239(1)	0.0248(2)	0.0252(1)	-0.92(2)	-0.97(4)	-0.97(2)
MEM	0.030(9)	0.025(2)	0.024(3)	-1(2)	-0.6(2)	-0.2(2)
DWA	n/a	0.08(4)	n/a	n/a	-6(2)	n/a
p-bits:2nd order (FPGA)	0.0194(1)	0.0206(2)	0.0210(3)	-3.70(4)	-3.76(6)	-3.74(2)
p-bits:3rd order (FPGA)	0.0182(6)	0.0201(2)	0.0202(1)	-4.13(6)	-4.30(0)	-4.23(1)

that can match the prefactor *and* the scaling of dedicated and expensive ASICs. The scalability of our system could be

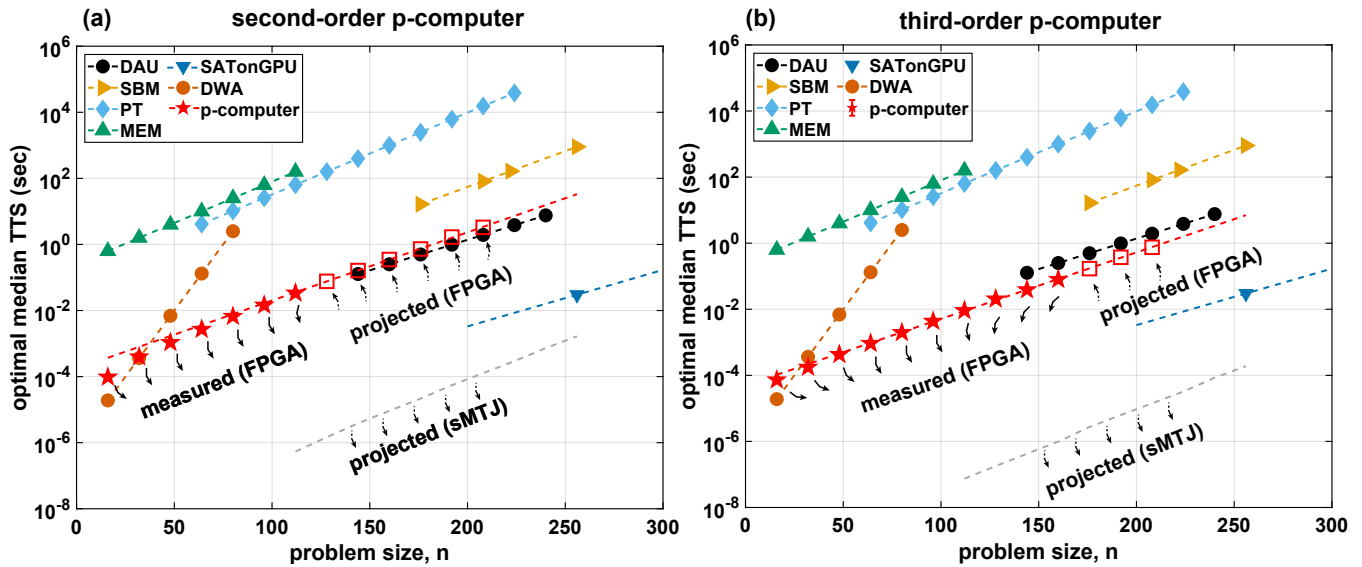


Fig. 7. Optimal median time to solution (TTS) for quartile $q = 0.5$ is shown as a function of problem size, n , for different state-of-the-art solvers: we adapt the figure from [10] for other solvers and add the results from the p-computer onto it. The solid red stars represent measured data for the FPGA-based p-computer. Hollow red squares indicate FPGA projections based on the CPU data from Figure 3. Error bars obtained from 95% confidence intervals are smaller than the size of the markers and omitted. The gray dashed line represents projections for stochastic Magnetic Tunnel Junction (sMTJ)-based p-computers (see the text).

improved significantly by the integration of larger or multiple FPGAs or using nanodevice-based p-computers, specifically, stochastic magnetic tunnel junctions (sMTJ) [19]. For such an sMTJ-based p-computer, detailed projections [19, 32] indicate that a capacity of $N = 10^6$ p-bits on a single chip is feasible, given that magnetic memory technology has already integrated up to *billions* of MTJs in CMOS-compatible chips [33]. In addition, an MC sweep time of $\tau = 1$ ns is also feasible and has been experimentally demonstrated [34]. Having $N = 10^6$ p-bits would allow fitting a significant number of parallel runs (e.g., $f_p(n) \approx 400$ for $n = 208$ for the second order and ≈ 1600 for the third order). With the prefactor being a function of n , the slope slightly increases to 0.0241 and 0.02375, respectively.

The greedy algorithm implemented by Ref. [17] still has the best experimentally obtained TTS; however, dedicated Ising solvers are closing the gap. Indeed, nanodevice implementations of p-bits could lead to orders of magnitude improvement over the state-of-the-art, motivating the engineering of such systems.

G. Assumptions and Qualifications

To maximize the transparency of our benchmarking approach, we collectively report all our assumptions and qualifications that have gone into producing our main result in Figure 7. While we do not entirely ignore replica swap computations, as we explain below, we do not include replica exchange times in our calculations, which are currently done by an external CPU that communicates with the FPGA. This is similar to earlier versions of the DAU [5]. However, this is not a fundamental problem, and future versions can perform on-chip replica swaps with custom logic as the newer DAU does [10]. To estimate replica swap times, we consider replica

exchanges as flipping all the spins in each replica. For each swap attempt, we add two full sweeps (each taking 66.67 ns) to our sweeps-to-solution calculations. This is a safe estimate as the on-chip replica swap can be performed at a much higher clock frequency, leading to lower swapping latencies. In such an implementation, the energy computation would be the costliest step, and we have achieved on-chip energy calculation latencies of approximately 56 ns for problem sizes up to $n = 256$. This is well below our two-sweep assumption. The only part that we have currently not considered is the probabilistic swap of β values with a single random number, and this can be achieved within a clock cycle or two. Our fully on-chip PT implementation will be discussed elsewhere. We have not accounted for read-write times between FPGA and external CPU in our TTS calculations since the APT algorithm does not require rewriting the weights, which is a one-time cost. Even though the reconfigurable sparse master graph approach we introduce houses multiple instances of a given size in a single FPGA synthesis, it does require a new synthesis at different sizes. This is not a fundamental problem either since, for custom ASIC implementations (for example, with sMTJs or digital CMOS), much larger problem sizes can be housed on-chip. The FPGA data pertains to sizes ranging from $n = 16$ to $n = 112$ for second-order and $n = 160$ for third-order. Projections beyond these sizes are based on the CPU emulation in Figure 3. The algorithmic sweeps to the solution are the same in both FPGA and CPU implementations, indicating our scaling factors are robust. Due to the limitations of the moderate FPGAs we used, at $n = 96$ and $n = 112$, we were constrained to fitting only 50 instances into our second-order master graphs. However, we carefully checked that for the chosen 50 instances, the success probabilities were identical to those obtained from

100 instances. For third-order master graph implementation, owing to a reduced hardware utilization, all 100 instances for all problem sizes till $n = 160$ were used for generating the FPGA data. In the implementation of the APT preprocessing algorithm for the third-order problems, we used exactly the same hyperparameters as those used for the second-order problems. This led to fewer replicas for third-order instances, which may have deteriorated the time-to-solution (but not the scaling). Tuning the parameters of APT to match the number of replicas in the second order may lead to further performance advantages in optimized designs.

III. CONCLUSION

In this paper, we have introduced a reconfigurable master graph architecture that can be useful to solve multiple instances of sparse optimization problems. Our master graph modifies neighbor connectivity, reproducing all-to-all reconfigurability for sparse problems while holding on to a highly efficient, massively parallel Gibbs sampling procedure based on asynchronous (and colored) clocks for both second-order as well as third-order interaction-based p-computers. We have implemented this architecture for FPGA-based probabilistic computers and shown excellent algorithmic and prefactor performance in the XORSAT challenge, where a number of leading custom-built Ising machines have recently been evaluated. We have also evaluated the performance of third-order p-computers for these problems and reported a significant prefactor advantage. Nanodevice-based implementations of p-computers may lead to much larger improvements at larger scales.

IV. METHODS

A. Third-order instance generation

We follow the following procedure to convert second-order XORSAT problems to third-order. For each auxiliary spin, find the product of all of its weights and bias. If this number is positive, then that XORSAT clause is of the form

$$m_1 \oplus m_2 \oplus m_3 = 1$$

Otherwise, the clause equals -1 . Then, for all non-auxiliary spins, we set the corresponding weight in the third-order tensor to ± 1 , equal to the literal to which the clause is equal. The resulting tensor is the weight tensor corresponding to the cubic form of the original XORSAT problem.

B. Bipolar to Binary Weight Conversion

As mentioned in Section II E 2, it is much more convenient to implement the MCMC algorithm in the FPGA in terms of binary variables, where $s_i \in \{0, 1\}$ and the random number lies in the interval $[0, 1]$. However, the weights for all orders of interactions need to be converted to their binary equivalents by following these equations after applying the standard map $m \rightarrow 2s - 1$ to bipolar variables m :

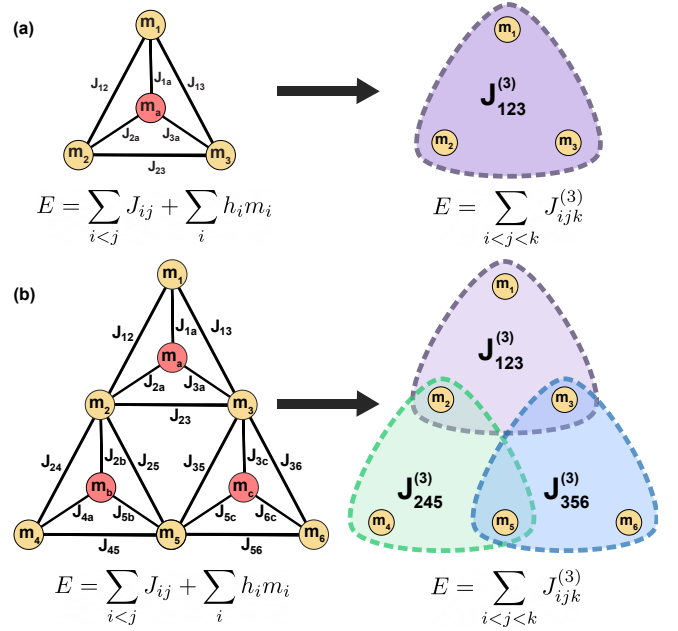


Fig. 8. a) A single XORSAT gadget is reduced into cubic form. The auxiliary spin is removed, and the 6-edge weights are replaced by a single weight. b) A 3-clause XORSAT problem is converted into cubic form. No spin is in more than three clauses.

$$J'_{ijk}{}^{(3)} = 8J_{ijk}{}^{(3)} \quad (9)$$

$$J'_{ij}{}^{(2)} = \sum_k (-4J_{ijk}{}^{(3)}) + 4J_{ij}{}^{(2)} \quad (10)$$

$$h'_i = \sum_{jk} J'_{ijk}{}^{(3)} - 2 \sum_j J'_{ij}{}^{(2)} + 2h_i \quad (11)$$

where $J_{ijk}{}^{(3)}$, $J_{ij}{}^{(2)}$ and h_i are the bipolar weights and biases, whereas $J'_{ijk}{}^{(3)}$, $J'_{ij}{}^{(2)}$ and h'_i are the binary weights and biases. It is interesting to note that the conversion to binary introduces second-order and bias terms even for a purely third-order problem in the bipolar form. Eq. 2 is also converted to its corresponding binary form:

$$s_i = \text{sgn} [\theta(\beta I'_i) - \text{rand}_U(0, 1)] \quad (12)$$

Here, $s_i \in \{0, 1\}$, θ is the Heaviside function implemented using a 32-bit lookup table (LUT), $\text{rand}_U(0, 1)$ is a 32-bit random number sampled from a uniform distribution between 0 and 1, generated using Xoshiro, and I'_i is the binary synapse.

C. Calculation of Optimal Median Time-to-Solution

For the calculation of TTS used in Eq. 7, we proceed exactly as described in [10]: once instance-wise success probabilities ($p_i(t_f)$) are estimated as a function of t_f , we calculate a $\text{TTS}_i(t_f) = t_f \ln(1 - 0.99) / \ln(1 - p_i(t_f))$. Then, we bootstrap the median (or the other quartiles) of $\text{TTS}_i(t_f)$ with 1000 samples. The mean of the bootstrapped distribution corresponds to $\langle \text{TTS}(t_f) \rangle_q$, whose minimum is $\langle \text{TTS} \rangle_q$.

Kowalsky *et al.* [10] calculate the $p_i(t_f)$ using a sophisticated approach; however, we adopt the same approach used in Figure 2: $p_i(t_f)$ is calculated over 1000 runs where t_f is measured up to a maximum of 3000 swap attempts. We found that both approaches produce exactly the same slope for p-computers and do not affect our comparisons.

DATA AVAILABILITY

All processed data generated in this study are provided in the main text. The data that supports the plots within this paper can be found in the GitHub repository mentioned in the code availability section. Other findings of this study are available from the corresponding authors upon reasonable request.

CODE AVAILABILITY

The CPU codes running the Adaptive Parallel Tempering algorithm and our raw data used to produce the lower panel of Figure 2, Figure 3 and Figure 7 can be found on the GitHub repository: <https://github.com/OPUSLab/XORSATwithpbits>

REFERENCES

- [1] Naeimeh Mohseni, Peter L McMahon, and Tim Byrnes. Ising machines as hardware solvers of combinatorial optimization problems. *Nature Reviews Physics*, 4(6):363–379, 2022.
- [2] Hao Lo, William Moy, Hanzhao Yu, Sachin Sapatnekar, and Chris H Kim. An ising solver chip based on coupled ring oscillators with a 48-node all-to-all connected array architecture. *Nature Electronics*, pages 1–8, 2023.
- [3] Ryan Hamerly, Takahiro Inagaki, Peter L McMahon, Davide Venturelli, Alireza Marandi, Tatsuhiro Onodera, Edwin Ng, Carsten Langrock, Kensuke Inaba, Toshimori Honjo, et al. Scaling advantages of all-to-all connectivity in physical annealers: the coherent ising machine vs d-wave 2000q. *Feedback*, 1:a2, 2018.
- [4] Hayato Goto, Kosuke Tatsumura, and Alexander R Dixon. Combinatorial optimization by simulating adiabatic bifurcations in nonlinear Hamiltonian systems. *Science advances*, 5(4):eaav2372, 2019.
- [5] Maliheh Aramon, Gili Rosenberg, Elisabetta Valiante, Toshiyuki Miyazawa, Hiroataka Tamura, and Helmut G Katzgraber. Physics-inspired optimization for quadratic unconstrained problems using a digital annealer. *Frontiers in Physics*, 7:48, 2019.
- [6] Tianshi Wang. Oscillators do the hard bits. *Nature Electronics*, pages 1–2, 2023.
- [7] Navid Anjum Aadit, Andrea Grimaldi, Mario Carpentieri, Luke Theogarajan, John M Martinis, Giovanni Finocchio, and Kerem Y Camsari. Massively parallel probabilistic computing with sparse Ising machines. *Nature Electronics*, 5(7):460–468, 2022.
- [8] Emile Aarts and Jan Korst. *Simulated annealing and Boltzmann machines: a stochastic approach to combinatorial optimization and neural computing*. John Wiley & Sons, Inc., 1989.
- [9] Itay Hen. Equation planting: a tool for benchmarking ising machines. *Physical Review Applied*, 12(1):011003, 2019.
- [10] Matthew Kowalsky, Tameem Albash, Itay Hen, and Daniel A Lidar. 3-regular three-xorsat planted solutions benchmark of classical and quantum heuristic optimizers. *Quantum Science and Technology*, 7(2):025008, 2022.
- [11] Navid Anjum Aadit, Masoud Mohseni, and Kerem Y Camsari. Accelerating adaptive parallel tempering with fpga-based p-bits. In *2023 IEEE Symposium on VLSI Technology and Circuits (VLSI Technology and Circuits)*, pages 1–2. IEEE, 2023.
- [12] Masoud Mohseni, Daniel Eppens, Johan Strumpf, Raffaele Marino, Vasil Denchev, Alan K Ho, Sergei V Isakov, Sergio Boixo, Federico Ricci-Tersenghi, and Hartmut Neven. Nonequilibrium monte carlo for unfreezing variables in hard combinatorial optimization. *arXiv preprint arXiv:2111.13628*, 2021.
- [13] Humberto Munoz Bauza and Daniel A. Lidar. Scaling Advantage in Approximate Optimization with Quantum Annealing. 2024. *arXiv preprint arXiv:2401.07184*.
- [14] John Aiken and Fabio L Traversa. Memcomputing for accelerated optimization. *arXiv preprint arXiv:2003.10644*, 2020.
- [15] Satoshi Matsubara, Motomu Takatsu, Toshiyuki Miyazawa, Takayuki Shibasaki, Yasuhiro Watanabe, Kazuya Takemoto, and Hiroataka Tamura. Digital annealer for high-speed solving of combinatorial optimization problems and its applications. In *2020 25th Asia and South Pacific Design Automation Conference (ASP-DAC)*, pages 667–672. IEEE, 2020.
- [16] Kelly Boothby, Paul Bunyk, Jack Raymond, and Aidan Roy. Next-generation topology of d-wave quantum processors. *arXiv preprint arXiv:2003.00133*, 2020.
- [17] Massimo Bernaschi, Mauro Bisson, Massimiliano Fatica, Enzo Marinari, Víctor Martin-Mayor, Giorgio Parisi, and Federico Ricci-Tersenghi. How we are leading a 3-xorsat challenge: From the energy landscape to the algorithm and its efficient implementation on gpus (a). *Europhysics Letters*, 133(6):60005, 2021.
- [18] Charlie Carlson, Daniel Frishberg, and Eric Vigoda. Improved distributed algorithms for random colorings. *arXiv preprint arXiv:2309.07859*, 2023.
- [19] William A Borders, Ahmed Z Pervaiz, Shunsuke Fukami, K. Y. Camsari, Hideo Ohno, and Supriyo Datta. Integer factorization using stochastic magnetic tunnel junctions. *Nature*, 2019.
- [20] Yihan He, Chao Fang, Sheng Luo, and Gengchiao Liang. Many-body effects-based invertible logic with a simple energy landscape and high accuracy. *IEEE Journal on Exploratory Solid-State Computational Devices and Circuits*, 2023.
- [21] Connor Bybee, Denis Kleyko, Dmitri E. Nikonov, Amir Khosrowshahi, Bruno A. Olshausen, and Friedrich T. Sommer. Efficient Optimization with Higher-Order Ising Machines. *arXiv preprint arXiv:2212.03426*, 2022.
- [22] T. Bhattacharya, G. H. Hutchinson, G. Pedretti, X. Sheng, J. Ignowski, T. Van Vaerenbergh, R. Beausoleil, J. P. Strachan, and D. B. Strukov. Computing High-Degree Polynomial Gradients in Memory. 2024. *arXiv preprint arXiv:2401.16204*.
- [23] Taro Kanao and Hayato Goto. Simulated bifurcation for higher-order cost functions. *Applied Physics Express*, 16(1):014501, 2022. ISSN 1882-0786. <http://dx.doi.org/10.35848/1882-0786/acaba9>. DOI 10.35848/1882-0786/acaba9.
- [24] Mohammad Hizzani, Arne Heitmann, George Hutchinson, Dmitrii Dobrynin, Thomas Van Vaerenbergh, Tinish Bhattacharya, Adrien Renaudineau, Dmitri Strukov, and John Paul Strachan. Memristor-based hardware and algorithms for higher-order Hopfield optimization solver outperforming quadratic Ising machines. 2023. *arXiv preprint arXiv:2311.01171*.

- [25] Yuqi Su, Tony Tae-Hyoung Kim, and Bongjin Kim. A Reconfigurable CMOS Ising Machine With Three-Body Spin Interactions for Solving Boolean Satisfiability With Direct Mapping. *IEEE Solid-State Circuits Letters*, 6:221–224, 2023. DOI 10.1109/LSSC.2023.3303332.
- [26] Yihan He, Chao Fang, Sheng Luo, and Gengchiao Liang. Logically Synthesized Invertible Logic Based on Many-body Effects with Probabilistic-bit Implementation. In *2023 Silicon Nanoelectronics Workshop (SNW)*, pages 39–40, 2023. DOI 10.23919/SNW57900.2023.10183978.
- [27] Yihan He, Chao Fang, Sheng Luo, and Gengchiao Liang. Many-Body Effects-Based Invertible Logic With a Simple Energy Landscape and High Accuracy. *IEEE Journal on Exploratory Solid-State Computational Devices and Circuits*, 9(2):83–91, 2023. DOI: 10.1109/JXCDC.2023.3320230
- [28] Shuvro Chowdhury, Kerem Y Camsari, and Supriyo Datta. Accelerated quantum monte carlo with probabilistic computers. *Communications Physics*, 6(1):85, 2023.
- [29] Shuvro Chowdhury, Andrea Grimaldi, Navid Anjum Aadit, Shaila Niazi, Masoud Mohseni, Shun Kanai, Hideo Ohno, Shunsuke Fukami, Luke Theogarajan, Giovanni Finocchio, et al. A full-stack view of probabilistic computing with p-bits: devices, architectures and algorithms. *IEEE Journal on Exploratory Solid-State Computational Devices and Circuits*, 2023.
- [30] Daniel Brélaz. New methods to color the vertices of a graph. *Communications of the ACM*, 22(4):251–256, 1979.
- [31] David Blackman and Sebastiano Vigna. Scrambled linear pseudorandom number generators. *ACM Transactions on Mathematical Software (TOMS)*, 47(4):1–32, 2021.
- [32] Brian Sutton, Rafatul Faria, Lakshmi Anirudh Ghantasala, Risi Jaiswal, Kerem Yunus Camsari, and Supriyo Datta. Autonomous probabilistic coprocessing with petaflips per second. *IEEE Access*, 8:157238–157252, 2020.
- [33] Sumio Ikegawa, Frederick B Mancoff, Jason Janesky, and Sanjeev Aggarwal. Magnetoresistive random access memory: Present and future. *IEEE Transactions on Electron Devices*, 67(4):1407–1419, 2020.
- [34] Keisuke Hayakawa, Shun Kanai, Takuya Funatsu, Junta Igarashi, Butsurin Jinnai, WA Borders, H Ohno, and S Fukami. Nanosecond random telegraph noise in in-plane magnetic tunnel junctions. *Physical Review Letters*, 126(11):117202, 2021.
- [35] Federico Ricci-Tersenghi. Being glassy without being hard to solve. *Science*, 330(6011):1639–1640, 2010. American Association for the Advancement of Science.

ACKNOWLEDGMENTS

This work has been supported by an ONR-MURI grant N000142312708 and the Semiconductor Research Corporation (SRC). Use was made of computational facilities purchased with funds from the National Science Foundation (CNS-1725797) and administered by the Center for Scientific Computing (CSC). The CSC is supported by the California NanoSystems Institute and the Materials Research Science and Engineering Center (MRSEC; NSF DMR 2308708) at UC Santa Barbara. We gratefully acknowledge discussions with Andrea Grimaldi, Giovanni Finocchio and Masoud Mohseni.

AUTHOR CONTRIBUTIONS

SN, SK, NAA, and KYC conceived the study. KYC supervised the study. SC, SK, and SN developed the higher-order p-bit mapping, graph and hypergraph coloring, and algorithms used. SN and NAA developed the all-to-all reconfigurable FPGA-based p-computer architecture. All authors have participated in discussing the results and helped improve the manuscript.

COMPETING INTERESTS

The authors declare no competing interests.